# Accurate Models of Collisions in Glow Discharge Simulations

W. N. G. Hitchon, *Member, IEEE,* G. J. Parker, and J. E. Lawler

*Abstract*—**Very detailed, self-consistent kinetic glow discharge simulations are used to examine the effect of various models of collisional processes. The effects of allowing anisotropy in elastic electron collisions with neutral atoms instead of using the momentum transfer cross-section, the effects of using an isotropic distribution in inelastic electron-atom collisions, and the effects of including a Coulomb electron-electron collision operator are all described. It is shown that changes in any of the collisional models, especially the second and third described above, can make a profound difference in the simulation results. This confirms that many discharge simulations have great sensitivity to the physical and numerical approximations used. Our results reinforce the importance of using a kinetic theory approach with highly realistic models of various collisional processes.**

## I. Introduction

SIMULATIONS of discharges inevitably incorporate simplified models of collisions and other physical processes. As more extensive tests of simulations are done, a consistent observation is that the predictions depend significantly on the exact models used to describe physical processes. In this paper, we examine models for three types of electron collisions, to determine their effect on discharge simulations. Models for collisions of electrons with neutral atoms, both elastic and inelastic, and Coulomb collisions between electrons, are studied. As might be expected, the way the collisions are handled can completely change the results of the simulation.

A critical examination of fluid simulations has shown that they are perhaps deceptively simple [1]. We have previously discussed an array of tests which we applied to the numerical simulations which we have developed to find particle distribution functions [2]. The need to vary all the discreteness parameters was emphasized, that is the time step and the mesh spacing in physical space and in velocity, to check that the simulation results are invariant as these are changed. Equally important, steps were taken to eliminate numerical diffusion as far as possible, either by changing the physical models or taking a longer time step $\Delta t$. Other sources of error are due to the finite mesh but might not be removed by reducing the mesh size within the practical range. These were addressed by changing the physical model and looking for differences in the results. The simulation results were also shown to be reasonable on the basis of a set of simple physical arguments.

For the rf discharge we studied, numerical diffusion was potentially a very serious problem but was reduced to a low level by various means. The scheme exactly conserved energy, and momentum was conserved to an accuracy dependent on the mesh. The mesh error in the momentum was shown to effect the results very little. Ways to increase $\Delta t$ were presented. Varying the spatial and velocity mesh had only small effects provided each was reasonably small.

An example of the caution which must be exercised arose in this testing process. The electron current density $J_e$ would vary slightly when the velocity mesh was altered, apparently because the flux of electrons is only known on the mesh to a fractional error of order $\Delta V/V$, where $\Delta V$ is the spacing of the velocity mesh and $V$ is the velocity. This was typically a small error. The electron temperature $T_e$ (defined such that $\frac{3}{2}k_B T_e$ is the average energy of a non-Maxwellian distribution) was found in some cases to follow very closely the drift tube data as $J_e$ varied. The behavior of $T_e$ was apparently 'physically' correct, in that $T_e$ agreed with drift tube data as $J_e$ was varied. Although $T_e$ still varied little, its fractional change was considerably bigger than $\Delta V/V$ because of shifts in the physical operating point. This set a limit on the $\Delta V/V$ which could be used.

In later work [3], the effect of allowing electron momentum to be conserved to a varying extent in inelastic collisions was considered, with surprisingly significant resultant changes. This implied the necessity of examining the use of the true angular distribution of scattered electrons in both elastic and inelastic collisions with neutral atoms. Coulomb collisions between electrons are included for their role in redistributing electron energy [4], [5]. They do not have a significant effect on the electron momentum balance, but for low energy electrons the competing process in the energy balance is energy transfer to atoms due to recoil in elastic collisions. This is quite slow and the weak Coulomb collision process plays an important role in balancing it. A simple and efficient Coulomb operator is described here and tested.

Section II describes the implementation of collision operators which allow electron momentum to be conserved to a varying extent in elastic and inelastic electron-neutral atom

Manuscript received January 20, 1994; revised April 20, 1994. This research is supported in part by the General Electric Company and in part by NSF grant number ECD-8721545.

W. N. G. Hitchon is with the Engineering Research Center for Plasma Aided Manufacturing, University of Wisconsin, Madison, WI 53706, USA.

G. J. Parker and J. E. Lawler are with the Department of Physics, University of Wisconsin, Madison, WI 53706, USA.

G. J. Parker is currently at Lawrence Livermore National Laboratory, Plasma Physics Research Institute, P.O. Box 808, L-418, Livermore, CA 94550 USA.

IEEE Log Number 9402570.

0093–3813/94$04.00 © 1994 IEEE

collisions. Section III describes how electrons are redistributed with an anisotropic distribution. Section IV describes the implementation of electron-electron Coulomb collisions. Results and conclusions are found in Section V.

## II. Elastic and Inelastic Collisions

### A. Elastic Collisions

Elastic collisions of electrons with neutral atoms are typically anisotropic in nature. A common assumption made by modellers of gas discharges is that use of the momentum transfer (MT) cross section is adequate. If this is used, the scattered electrons are redistributed isotropically in velocity-space. In this section we consider the use of the total elastic cross section, in which case an anisotropic redistribution of electrons must be done. We then examine the effect on discharge simulations.

We start with the differential cross section for elastic scattering. The differential cross section only depends on the initial relative velocity between the electron and neutral atom and the angle through which the electron is scattered, $\theta'$, from its initial velocity (see Fig. 1). The azimuthal scattering angle is uniformly distributed, so we are only concerned with the polar angle to which the electron is scattered.

In our model, the average relative energy between the electron and the scattering neutral atom is given by

$$\tau_0 = \frac{1}{2}\frac{mM}{m+M}[V_0^2 + 3k_B T_g/M], \tag{1}$$

where $m$ and $M$ are the masses of the electron and neutral atom, respectively, $k_B$ is Boltzmann's constant, $T_g$ is the temperature of the neutral atoms and $\vec{V}_0$ is the electron's initial velocity. We now construct the average cosine of the angle scattered, $\overline{\mu'(\tau_0)} \equiv \overline{\cos\theta'}$, from

$$\overline{\mu'(\tau_0)} = \frac{\displaystyle\int_{-1}^{1} \mu' \frac{d\sigma(\tau_0)}{d\mu'} d\mu'}{\displaystyle\int_{-1}^{1} \frac{d\sigma(\tau_0)}{d\mu'} d\mu'}, \tag{2}$$

where $d\sigma(\tau_0)/d\mu'$ is the differential cross section, and the total cross section is given by

$$\sigma(\tau_0) = \int_{-1}^{1} \frac{d\sigma(\tau_0)}{d\mu'} d\mu'. \tag{3}$$

We note that the definition of the momentum transfer cross section, $\sigma^{MT}(\tau_0)$ can be expressed in terms of $\overline{\mu'(\tau_0)}$ as

$$\begin{aligned}\sigma^{MT}(\tau_0) &= \int_{-1}^{1} (1-\mu') \frac{d\sigma(\tau_0)}{d\mu'} d\mu' \\ &= \sigma(\tau_0)(1 - \overline{\mu'(\tau_0)}).\end{aligned} \tag{4}$$

We emphasize that we will use $\sigma(\tau_0)$ to determine the collision rate, and in most cases $\sigma(\tau_0) > \sigma^{MT}(\tau_0)$.

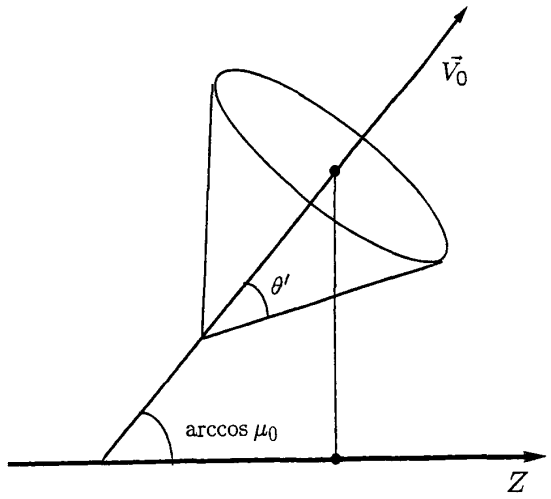


Fig. 1. Schematic for computing $\overline{V_{zf}}$ for elastic collisions.

The speed of the electron will on average change due to elastic recoil cooling, to a value given by

$$V_f = \cdot \left[V_0^2 - (1 - \overline{\mu'(\tau_0)})\frac{4}{M}\left(\frac{1}{2}mV_0^2 - \frac{3}{2}k_B T_g\right)\right]^{1/2}. \tag{5}$$

One can define an average final velocity along the initial velocity of the electron by $\overline{\mu'(\tau_0)}V_f$. Similarly, if the cosine of the angle between the initial velocity and, say, the $Z$ axis is given by $\mu_0$, then the component of the final velocity along the $Z$ axis is given on average over particles with the same initial velocity by $V_{zf} = \mu_0\overline{\mu'(\tau_0)}V_f$.

However, the set of electrons which have this final velocity $\vec{V}_f$ generally have different $\mu_0$. We construct an average $\mu_0$ such that $\overline{\mu_0}$ is an average over the electrons which have been scattered to the final speed $V_f$. Then, the average component of the final velocity along the $Z$ axis for the set of electrons is given by

$$\overline{V_{zf}} = \overline{\mu_0}\overline{\mu'(\tau_0)}V_f. \tag{6}$$

This quantity, which is proportional to the average $Z$ momentum of electrons at speed $V_f$ after an elastic collision is used to redistribute the scattered electrons with an anisotropic distribution (see Section III below).

Since elastic collisions are an important collision process in the discharges considered here, it was shown [2] that special care must be taken to ensure numerical diffusion is minimized. The appendix describes an equivalent "simplified elastic collision operator" which approximates the "full" collision operator described in the Section III. This simplified operator not only reduces numerical diffusion, but is computationally efficient.

### B. Inelastic Collisions

Unlike elastic electron-neutral atom collisions, differential cross sections are not readily available for inelastic electron-

neutral atom collisions, though the situation is improving [6], [7]. The lack of this information led us to introduce a parameter $h$ which is the fraction of the maximum possible $Z$ momentum of the electron(s) which is conserved in inelastic collisions (including ionizing collisions).

Again, we start by considering an electron with initial velocity $\vec{V}_0$ which makes an angle $\cos^{-1}(\mu_0)$ with respect to the $Z$ axis. After the collision, the electron will have a different final speed given by

$$V_f = \left(V_0^2 - \frac{2\tau_g}{m}\right)^{1/2}, \tag{7}$$

where $\tau_k$ is the energy given up in the collision. The average final velocity component along the $Z$ axis for this set of electrons is given by

$$\overline{V_{zf}} = h\overline{\mu_0}V_f, \tag{8}$$

where $h$ is a constant which represents the fraction of available linear momentum of electron(s) which is conserved during inelastic collisions. The parameter $h$, which replaces $\overline{\mu'(\tau_0)}$ in (6) for elastic scattering, is assumed to be independent of $\tau_0$ in (8) for inelastic scattering. (If more information was available on angular distributions from inelastic scattering, we could construct an energy dependent $h$. It would, based on simple physical arguments, vary from near zero at threshold energies to near unity at high energies.) Again, $\overline{\mu_0}$ is the average initial $\mu_0$ of the electrons which scatter to the final speed $V_f$.

For ionization, the final speed of each electron is determined by the differential cross section. Once the final speed of each electron is determined, the corresponding $\overline{V_{zf}}$ can be computed for each.

The next section describes how $\overline{V_{zf}}$ is used to redistribute the scattered electrons back onto the computational grid.

## III. Implementation of Angular Distributions of Scattered Particles

In Section II above, we constructed the quantity $\overline{V_{zf}}$ according to the type of collision the electron underwent. Specifically, $\overline{V_{zf}}$ is a double projection and average of the final velocity $\overline{V_f}$. First it is projected onto the initial velocity vector, using either the average of the cosine of the scattering angle $\mu'(\tau_0)$ or the adjustable parameter $h$. This projection is then again projected onto the $Z$ axis by using $\overline{\mu_0}$, the average initial $\mu_0$ of the electrons which scattered to the final speed $V_f$.

We redistribute the electrons back onto the computational grid using a two term Legendre polynomial for the angular distribution, so that $\overline{V_{zf}}$ and, of course, the number of electrons are conserved. The distribution of scattered electrons with respect to $\mu$ is $f(\mu) = \frac{1}{2}(1 + \alpha\mu)$. The first Legendre polynomial gives an isotropic distribution. It is now required to find the coefficient of the second polynomial, $\alpha$. Conservation of $\overline{V_{zf}}$ requires that

$$\overline{V_{zf}} = \tfrac{1}{2}\int_{-1}^{1} V_f\mu(1 + \alpha\mu)\, d\mu \tag{9}$$

(the factor of 1/2 is for normalization). Solving for $\alpha$, we find

$$\alpha = \frac{3\overline{V_{zf}}}{V_f}. \tag{10}$$

The above redistribution ensures equipartion but becomes negative if $|\alpha| \geq 1$. If $|\alpha| > 1$, i.e. $|\overline{V_{zf}}/V_f| > 1/3$, we then restrict the range of $\mu$ in which the electrons are redistributed so that both $\overline{V_{zf}}$ and electron number can be conserved with a positive electron density. For $\overline{V_{zf}} > 0$, we let the lower limit of integration be $\mu_l$, and now use $f(\mu) = 2(\mu - \mu_l)/(1 - \mu_l)^2$. To determine $\mu_l$ we require that $\overline{V_{zf}}$ be conserved. We find

$$\mu_l = 3\overline{V_{zf}}/V_f - 2. \tag{11}$$

In summary, if $|\overline{V_{zf}}/V_f| \leq 1/3$ then the electrons are redistributed using $f(\mu) = \frac{1}{2}(1 + (3\overline{V_{zf}}/V_f)\mu)$ over the full range of polar angles. Otherwise they are redistributed using $f(\mu) = 2(\mu - \mu_l)/(1 - \mu_l)^2$ in a limited range of polar angles. Both cases conserve electron number and $\overline{V_{zf}}$.

It is of interest to compare the two term Legendre distribution used here to another popular angular distribution, $1/[1+g(\tau_0)(1-\mu)]$ where $g(\tau_0) \ll 1$ for low $\tau_0$ and $g(\tau_0) \gg 1$ for high $\tau_0$. This distribution has been used extensively in Monte Carlo and PIC-Monte Carlo simulations [8]–[10]. Both approximations reproduce a known total elastic scattering cross section. If a good choice is made for $g(\tau_0)$, then both approximations reproduce a known elastic momentum transfer cross section. Indefinite integrals are analytic and are easily inverted for both distributions. This feature is important in Monte Carlo simulations. The two term Legendre distribution used here is somewhat less effective at reproducing details of the well known differential cross section for electron-Helium elastic scattering [11]. However our results from simulations at high reduced fields in the cathode fall region are most sensitive to the assumed angular distribution for inelastic electron-atom scattering. Either of the angular distributions is a reasonable approximation because these true angular distributions for the inelastic collisions are not well known. More legendre polynomials would be used if desired.

As mentioned above a simplified version, which exactly conserves particles and energy on the mesh, of this full elastic scattering operator is discussed in the appendix.

## IV. Electron-Electron Coulomb Collisions

In this section, we describe an efficient approximation suitable for electron-electron collisions. Coulomb collisions, by their nature, are computationally expensive to implement in a numerical simulation. It is often suggested that at the plasma densities and temperatures studied here, Coulomb colisions are not important in determining most macroscopic properties of the discharge. We are not concerned with the effects that Coulomb collisions have on the angular distribution of electrons, since electron-neutral atom collisions are believed to dominate that. We are concerned only with the energy transfer between 'cold' and 'hot' electron components that are found in the negative glow of dc discharges and in the "bulk" plasma of rf discharges.

It is common in gaseous electronics to find electron distribution functions which can be approximated as two Maxwellians. The basic approach described below can easily be adapted to model the effect of electron-electron Coulomb collisions on a distribution function which is approximately two or more Maxwellians. Simple analytic formulas can be used to compute energy transfer between pairs of Maxwellian distributions or between a beam distribution and a Maxwellian [4]. Coulomb collisional relaxation of a distinctly non-Maxwellian distribution, which could not be satisfactorily approximated as a set of Maxwellians or beams, might be better described using a more sophisticated Fokker-Planck approximation.

We start with Longmire's formula [4] which gives the rate of energy transfer between two Maxwellian distributions:

$$\frac{d(\frac{3}{2}k_BT_1)}{dt} = 4\left(\frac{2\pi}{mk_B}\right)^{1/2}\mathcal{N}_2e^4 \cdot \frac{T_2 - T_1}{(T_2+T_1)^{3/2}}\ln(2/\theta_m) \tag{12}$$

where $T_1$ and $T_2$ are the temperatures of the two Maxwellians, $e$ is the elementary electric charge (esu) and $\mathcal{N}_1$ and $\mathcal{N}_2$ are the densities of electrons in each Maxwellian. Here $\ln(2/\theta_m)$ is the Coulomb logarithm. Conservation of energy implies

$$\mathcal{N}_1\frac{d(\frac{3}{2}k_BT_1)}{dt} = -\mathcal{N}_2\frac{d(\frac{3}{2}k_BT_2)}{dt}. \tag{13}$$

The above formulae give two new Maxwellians at slightly different temperatures $T_1'$ and $T_2'$ after a time step $\Delta$t.

We have implemented Longmire's formula by fitting two or more Maxwellians to the actual electron distribution function. The fit is achieved by varying the initial temperatures ($T_1$ and $T_2$) until the residual is minimized. Once the initial temperatures are found, the new temperatures are computed from (13). In principle, the (normalization) coefficients of the Maxwellians are known; they are the initial values. However, we still have to determine small corrections to the coefficients for these Maxwellians in such a way as to ensure exact conservation properties on the mesh.

The constraints on the coefficients are that electron density and total energy are conserved. We define $\zeta_i$ as the fractional change of electron density in the computational cell $i$:

$$\zeta_i = \frac{\Delta n_i}{n_i}, \tag{14}$$

where $n_i$ is the initial density of electrons in the computational cell $i$ and $\Delta n_i$ is the change in density. This is proportional to the change in densities predicted by the Maxwellians, over the initial density they predict,

$$\zeta_i = \left(\frac{A_2n_2' + A_1n_1' - n_2 + n_1}{n_2 + n_1}\right)_i, \tag{15}$$

where $(n_1 + n_2)_i$ is the density of electrons that the initial Maxwellians give for this cell, $(n_1' + n_2')_i$ is the density the new Maxwellians give with the temperatures $T_1'$ and $T_2'$ and the initial coefficients, and $(A_1n_1' + A_2n_2')_i$ is the density that the new Maxwellians give, with $A_1, A_2$ the undetermined modifiers to the initial coefficients. $A_1$ and $A_2$ represent small corrections and thus should be close to unity.

Applying the constraints of number and energy conservation, we have

$$\sum_i \zeta_i n_i = 0 = A_1\sum_i n_i\left(\frac{n_1'}{n_2+n_1}\right)_i + A_2\sum_i n_i\left(\frac{n_2'}{n_2+n_1}\right)_i - \sum_i n_i \tag{16}$$

and

$$\sum_i \tau_i\zeta_i n_i = 0 = A_i\sum_i \tau_i n_i\left(\frac{n_1'}{n_2+n_1}\right)_i + A_2\sum_i \tau_i n_i\left(\frac{n_2'}{n_2+n_1}\right)_i - \sum_i n_i\tau_i \tag{17}$$

where the summations run over the velocity cells at fixed spatial location, $\tau_i$ is the kinetic energy associated with cell $i$, and $\Sigma_i\, n_i$ and $\Sigma_i\, n_i\tau_i$ are the density and total energy density of the initial electron distribution function, respectively. The above two equations are then used to compute $A_1$ and $A_2$. The change in density in cell $i$ is then simply $\zeta_i n_i$, which, by construction, conserves particle number and energy at that spatial location. It can be seen that this scheme has the essential property that, as $T_1'$ approaches $T_1$ and $T_2'$ approaches $T_2$, the change in the distribution goes smoothly to zero.

## V. Results and Conclusion

In the preceding sections, we have shown how we implement a) angular distributions for electron scattering off neutral atoms and b) energy transfer between electrons. In this section, we show what effects these collisions have on a dc discharge simulation.

First, however, in Fig. 2 we show an example of the effect of Coulomb collisions on a nonMaxwellian electron distribution function. (The dc discharge simulation is not appropriate in the absence of these Coulomb collisions, so a comparison to a dc discharge without Coulomb collisions is not made here.) In this case, the initial distribution is a sum of two Maxwellians initially at 1 and 5 eV with equal numbers of electrons in each (curve 1). Curves 2 and 3 show the distribution function after 1.75 and 9 microseconds, respectively. Integrating (13) shows that the rate of energy transfer is given correctly. The coldest electrons are heated while the hot tail electrons are cooled to fill in the 'bend' in the initial distribution.

We now turn to the full dc discharge simulation.

The dc discharge modelled here is summarized in Table I. It is a one dimensional discharge in helium between plane parallel electrodes. The processes and cross sections included here are similar to those described in ref. 12, except for the simplified elastic collision operator, the inclusion of Coulomb collisions, and anisotropic scattering. The flux of secondary electrons emitted from either electrode is $\Gamma_e = \gamma\Gamma_i$, where $\Gamma_i$ is the flux of ions into the electrode. $\gamma = 0.25$ was used here. Ion transport at a gas pressure of 3.5 Torr is dominated by charge-exchange. This cross section [13] was adjusted (increased) at low energy to reproduce measured ion mobilities [14] and thus compensate for neglecting elastic ion-neutral scattering.

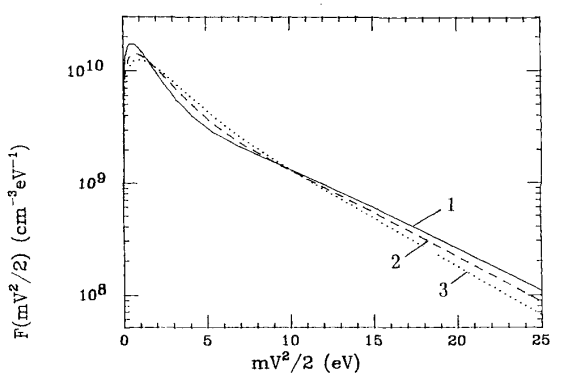


Fig. 2. Coulomb collision results. Curve 1: initial distribution, curve 2: $t = 1.75\,\mu$seconds, curve 3: $t = 9\,\mu$seconds. See text for initial distribution parameters.

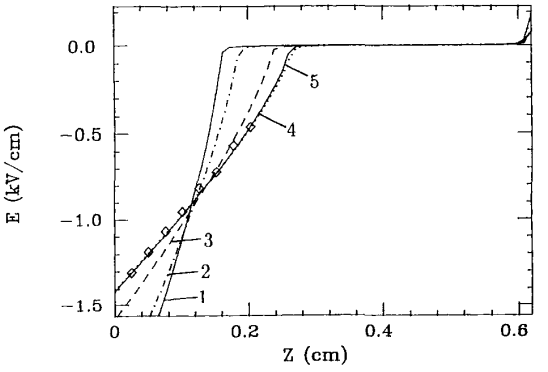


Fig. 3. Electric field. Curve 1: $h = 0$, elastic- MT, curve 2: $h = 0$, elastic-anisotropic, curve 3: $h = 1/2$, elastic- MT, curve 4: $h = 1$, elastic- MT, curve 5: $h = 1$, elastic- anisotropic.

TABLE I
VARIOUS DISCHARGE PARAMETERS USED IN THE SIMULATION

| Quality | Value | Units |
|---|---|---|
| He gas density | 10.8 | $10^{16}$ cm$^{-3}$ |
| neutral temperature | 350 | K |
| voltage | 211 | V |
| discharge length | 0.62 | cm |

A variety of inelastic and elastic electron-atom collisions are important. Direct or single-step ionization of ground state atoms and excitations of ground state atoms to the $n^1S, n^3S, n^1P, n^3P, n^1D$, and $n^3D$, levels where the principal quantum number $n \leq 5$, are included using the semiempirical cross sections of Alkhazov [15]. We note here that the cross section for $2^1P$ excitation from the ground state was taken from the plot, not the formula, in ref. [15]. The two outgoing electrons from single-step ionization share the available energy according to the differential cross section [15]. A superelastic collision is also included, namely the conversion of singlet to triplet metastable atoms $[\mathrm{He}(2^1S) + e^- \rightarrow \mathrm{He}(2^3S) + e^- + 0.80\,\mathrm{eV}]$ in collision with low-energy electrons. The cross section given by Phelps [16] with electron energy dependence from Fon *et al.* [17] is used. The elastic momentum transfer cross section and total cross sections are calculated from the differential elastic cross section of LaBahn and Callaway [11].

The metastable calculation has also been described by Sommerer *et al.* [12] Excitations to all triplet levels are assumed to cascade to the metastable $2^3S$ level. The singlet manifold is more complex because of the optically allowed transitions from the $n^1P$ levels to ground state. Transitions to the ground state are trapped. Here, natural and pressure broadening of the transitions dominate the trapped decay rate. The formula for the pressure broadening coefficient is from Corney [18]. Trapped radiative decay rates are calculated using analytic formulas for infinite-slab geometery [19], and vacuum decay rates [20] are used between excited levels.

The diffusion equation adequately describes transport of metastable atoms. The source rates per unit volume for singlet and triplet metastable atoms are found by the electron collision operator for each spatial location. Other contributions to the balance equations include metastable-metastable atom collisions, giving a ground state atom, an ion, and an electron with the appropriate energy [21]. Singlet metastable atoms' destruction in binary collisions with ground state atoms is also included [16].

Fig. 3 shows the electric field generated by the simulation. Curves 3 and 4 have been published previously [3], and the reader is referred there for more detailed comparison with experimental results. The diamonds are experimental electric fields from den Hartog, *et al.* [10]. Looking first at the effects of elastic electron collisions (curves 1, 2, 4 and 5), we see that the electric field is not greatly affected if the elastically scattered electrons are isotropically (using the momentum transfer cross section) or anisotropically redistributed (using the total cross section). The latter does seem to extend the Cathode Fall (CF) length and decrease the magnitude of the electric field at the cathode slightly. On the other hand, conserving electron momentum in inelastic collisions has a pronounced effect on the CF length and field magnitude. Specifically, as $h$ approaches 1, better agreement is found. These results are reasonable since the average energy in the CF is typically much larger than the excitation energies and the reduced electric field ($E/N$, $N$ being the density of ground state atoms) is a few thousand Townsends.

Fig. 4 shows the average electron energy in the same discharge. For completeness, the same cases are shown here as in Fig. 3. The gross features are as expected: high average electron energy in the CF and low average electron energy in the negative glow (NG). All these simulations have electron-electron Coulomb collisions. If we do not include Coulomb collisions, the electrons in the NG (whose density is many orders of magnitude larger than the density in the CF) cool down close to the neutral gas temperature due to elastic recoil cooling. Coulomb collisions allow the 'hot' group of electrons from the CF to transfer some of their energy to the trapped 'cold' electrons in the NG before they escape to the anode. (Comparison to a run without Coulomb collisions would not be appropriate, therefore.) The two cases which produced the 'correct' electric field (curves 4 and 5) give

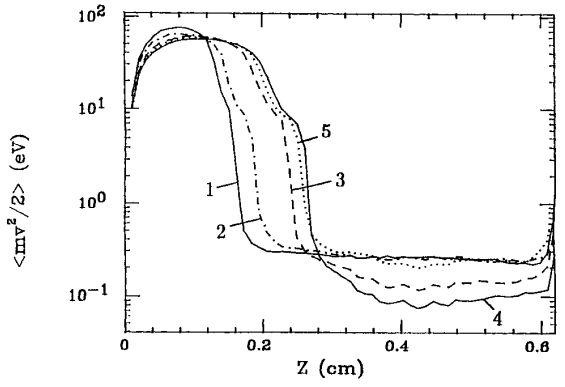


Fig. 4. Average electron energy. Curves are the same as Fig. 3.

different average electron energies in the NG. Specifically, using anisotropic scattering from elastic collisions instead of the isotropic momentum transfer cross section increases the average energy.

This is probably because the use of the momentum transfer cross section reduces the number of electrons scattered at higher energies (above ~15 eV). These electrons are then more likely to reach the anode sheath and escape the discharge.

Similar simulations were done for rf He glow discharges, as described previously [5]. Electron-electron Coulomb collisions and anisotropic angular distributions were included and compared to the original work for various rf driving voltages. At all driving voltages, no macroscopic quantity changed by more than 5% as quoted in ref. 5. This is of no surprise, since Coulomb collisions are not expected to be important for these low electron densities, and rf sheaths do not in these cases substain the discharge in a similar manner to the way the CF does for a dc discharge.

In conclusion, we have shown that including the angular distributions of electrons which have suffered elastic and inelastic collisions has a pronounced effect on dc discharge simulations. Inelastic collisions determine the CF length and magnitude of the electric field at the cathode. Anisotropic elastic collisions have a similar, though smaller, effect and also keep the NG electrons warmer compared to isotropic elastic scattering based on the momentum transfer cross section. Electron-electron Coulomb collisions are found to be essential for determining the correct average electron energy in the NG. The Coulomb operator presented here conserves both energy and electron number at a point in space and is computationally efficient.

## VI. Appendix
### The Simplified Elastic Collision Operator

We now describe the "simplified elastic collision operator." Like the operator introduced previously for isotropic scattering [2], this operator redistributes particles only to cells having the exactly correct total speed. Within that group of cells it attempts to redistribute particles in such a way as to ensure equipartition of energy. Subject to both of these requirements, it then attempts to conserve $\overline{V_{zf}}$.

The meshes used for each component of velocity $(V_z, V_\perp)$ are identical. A group of cells that have the same total speed are then given by $(V_z(\pm j), V_\perp(i))$ and $(V_z(\pm i), V_\perp(j))$, where $i$ and $j$ are integer indices. A group can consist of four cells, three cells (either $i$ or $j$ equal to zero), or two cells ($i = j$). This operator attempts to redistribute elastically scattered electrons between the cells in a group with no numerical diffusion in energy and exact conservation of $\overline{V_{zf}}$.

The total density of electrons scattering in a time step $\Delta t$ is given by

$$n_{scat} = \nu_{el}\Delta t \sum_l n_l, \tag{A1}$$

where $\nu_{el}$ is the elastic collision frequency, the sum runs over the cells in a group and $n_l$ is the initial density of electrons in cell $l$. Note that $\pm i, \pm j$ indices are represented by $l$. As we did for the full collision operator, we compute the final average velocity along the $Z$ axis for this group from

$$\overline{V_{zf}} = \overline{\mu'(\tau_o)} V_0 \sum_l \mu_l n_l / \sum_l n_l, \tag{A2}$$

where $\overline{\mu'(\tau_0)}$ is the average cosine of the scattering angle, $V_0$ is the initial speed associated with the group and $\mu_l$ is $V_z/V_0$ for cell $l$. Note that $\Sigma_l \mu_l n_l / \sum_l n_l$, is equivalent to $\overline{\mu_0}$ in (6). We assume that the redistribution of the scattered particles can be described by a two term Legendre expansion, $f(\mu) = \frac{1}{2}(1 + \alpha\mu)$, with $\alpha$ given by (10). To find the density going to each cell in the group, we take moments of the distribution until we have a closed set of equations.

Specifically, the zeroth moment conserves particle number in the group and is considered to be highest priority. The second moment (i.e. $\mu^2$) ensures equipartition of energy and is considered the next highest priority. The first moment ($\mu$) describes conservation of $Z$ momentum and is given third priority. Finally, the third moment ($\mu^3$) is used to close the system of equations and is given the lowest priority.

For a group with four cells, the fraction of scattered particles to each final cell where $l = a, b, c$, or $d$ (see Fig. 5a) is found to be

$$n'_a/n_{scat} = \frac{\mu_a(1/3 - \mu_b^2) + \alpha(1/5 - \mu_b^2/3)}{2\mu_a(\mu_a^2 - \mu_b^2)} \tag{A3}$$

$$n'_b/n_{scat} = \frac{\mu_b(\mu_a^2 - 1/3) + \alpha(\mu_a^2/3 - 1/5)}{2\mu_b(\mu_a^2 - \mu_b^2)} \tag{A4}$$

$$n'_c/n_{scat} = \frac{\mu_b(\mu_a^2 - 1/3) - \alpha(\mu_a^2/3 - 1/5)}{2\mu_b(\mu_a^2 - \mu_b^2)} \tag{A5}$$

$$n'_d/n_{scat} = \frac{\mu_a(1/3 - \mu_b^2) - \alpha(1/5 - \mu_b^2/3)}{2\mu_a(\mu_a^2 - \mu_b^2)}, \tag{A6}$$

where $\mu_a^2 + \mu_b^2 = 1$ and all $\mu$ are defined in Fig. 5.

For a group with three cells as shown in Fig. 5b, only the first three moments of the distribution are used. This results in the following fractions:

$$n'_a/n_{scat} = (1 + \alpha)/6 \tag{A7}$$

$$n'_b/n_{scat} = 2/3 \tag{A8}$$

$$n'_c/n_{scat} = (1 - \alpha)/6. \tag{A9}$$

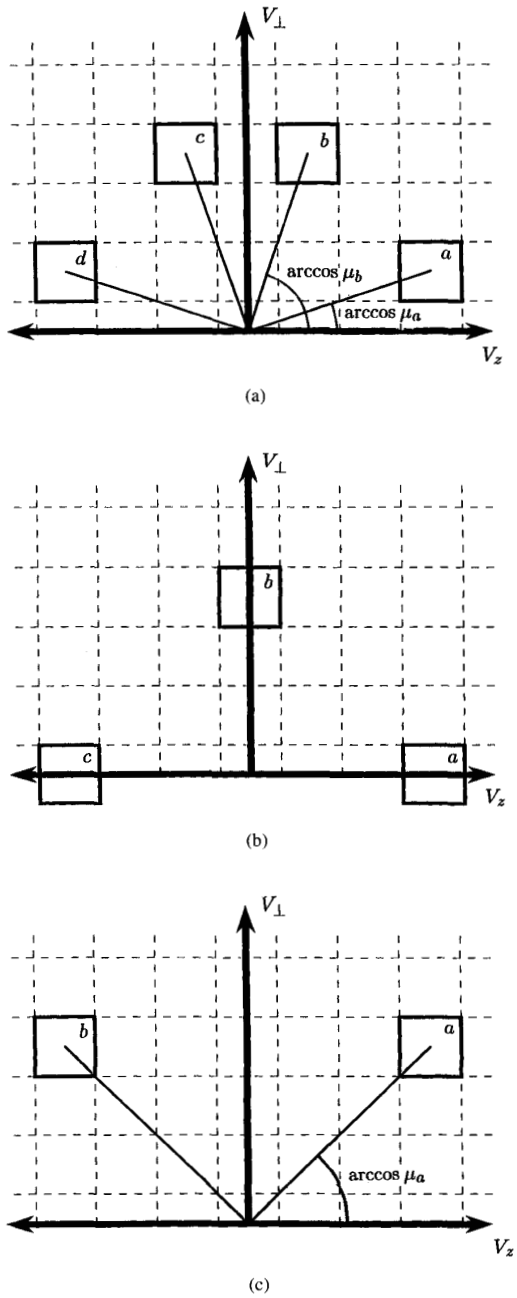


Fig. 5. (a) Schematic of simplified elastic collision operator with four cells. (b) Schematic of simplified elastic collision operator with three cells. (c) Schematic of simplified elastic collision operator with two cells.

Finally, if there are only two cells in a group as shown in Fig. 5c, then the zeroth and first moments (since the second moment can not be conserved in these groups) give

$$n'_a/n_{scat} = \frac{1}{2} + \frac{\alpha}{6\mu_a} \tag{A10}$$

$$n'_b/n_{scat} = \frac{1}{2} - \frac{\alpha}{6\mu_a}. \tag{A11}$$

If, for a given group, one (or more) of the fractions is less than zero, the most negative fraction is set equal to zero (which is always the cell with the largest $V_z$ in the opposite direction to $\overline{V}_{zf}$), and the remaining fractions are computed in a similar manner, but using one fewer moment of the distribution.

For a group of four cells, we find:

$$n'_a/n_{scat} = \frac{1/3 - \mu_b^2}{\mu_a^2 - \mu_b^2} \tag{A12}$$

$$n'_b/n_{scat} = \frac{3\mu_a\mu_b - 1}{6\mu_b(\mu_a - \mu_b)} + \frac{\alpha}{6\mu_b} \tag{A13}$$

$$n'_c/n_{scat} = \frac{3\mu_a\mu_b + 1}{6\mu_b(\mu_a + \mu_b)} - \frac{\alpha}{6\mu_b} \tag{A14}$$

$$n'_d/n_{scat} = 0. \tag{A15}$$

If any of these fractions are less than zero, we use for a group of four cells the zero and first moment (since the second moment can not be satisfied) and we find:

$$n'_a/n_{scat} = 0 \tag{A16}$$

$$n'_b/n_{scat} = \frac{1}{2} + \frac{\alpha}{6\mu_b} \tag{A17}$$

$$n'_c/n_{scat} = \frac{1}{2} - \frac{\alpha}{6\mu_b} \tag{A18}$$

$$n'_d/n_{scat} = 0. \tag{A19}$$

In a group of three cells with a negative fraction, we use the zero and second moments to find

$$n'_a/n_{scat} = 1/3 \tag{A20}$$

$$n'_b/n_{scat} = 2/3 \tag{A21}$$

$$n'_c/n_{scat} = 0. \tag{A22}$$

This operator is used in the simulations reported here which use elastic collisions with $\overline{V_{zf}}$ conservation. The simplified operator does not include elastic recoil cooling, but it does transfer momentum without numerical diffusion of particles in speed (or energy). Additional elastic recoil cooling is included in the full elastic scattering operator to compensate for the neglect of it in the simplified operator. Typically, after 499 executions of the simplified operator the full operator is executed with 500 times the rate of elastic recoil cooling.

## REFERENCES

[1] M. H. Wilcoxson and V. I. Manousiouthakis, "Well-posednes of continuum models of weakly ionized plasmas," *IEEE Trans. Plasma Sci.*, vol. 21, p. 213, 1993.

[2] W. N. G. Hitchon, G. J. Parker, and J. E. Lawler, "Physical and numerical verification of discharge calculations," *IEEE Trans. Plasma Sci.*, vol. 21, p. 228, 1993.

[3] G. J. Parker, W. N. G. Hitchon, and J. E. Lawler, "Self-consistent kinetic model of an entire dc discharge," *Phys. Lett. A*, vol. 174, p. 308, 1993.

[4] C. L. Longmire, *Elementary Plasma Physics*. New York: Wiley, 1963, p. 204.

[5] G. J. Parker, W. N. G. Hitchon, and J. E. Lawler, "Kinetic modeling of the $\alpha$ to $\gamma$ transition in rf discharges," *Phys. Fluids B*, vol. 5, p. 646, 1993.

[6] S. Jones, D. H. Madison, and M. K. Srivastava, "Near-threshold ionization of hydrogen and helium by electron impact," *J. Phys. B*, vol. 25, p. 1899, 1992.

[7] T. Rösel, J. Röder, L. Frost, K. Jung, H. Ehrhardt, S. Joines, and D. H. Madison, "Absolute triple differential cross section for ionization of helium near threshold," *Phys. Rev. A*, vol. 46, p. 2539, 1992.

[8] M. Surendra, D. B. Graves, and I. J. Morey, "Electron heating in low-pressure rf glow discharges," *Appl. Phys. Lett.,* vol. 56, p. 1022, 1990.
[9] M. Surendra, D. B. Graves, and G. M. Jellum, "Self-consistent model of a direct-current glow discharge: Treatment of fast electrons," *Phys. Rev. A,* vol. 41, p. 1112, 1990.
[10] E. A. den Hartog, D. A. Doughty, and J. E. Lawler, "Laser optogalvanic and fluorescence studies of the cathode region of a glow discharge," *Phys. Rev. A,* vol. 38, p. 2471, 1988.
[11] R. W. LaBahn and J. Callaway, *Phys. Rev.,* vol. 2, p. 366, 1970; *Phys. Rev. A,* vol. 180, p. 91, 1969; vol. 188, p. 520, 1969.
[12] T. J. Sommerer, W. N. G. Hitchon, R. E. P. Harvey, and J. E. Lawler, "Self-consistent kinetic calculations of helium rf discharges," *Phys. Rev. A,* vol. 43, p. 4452, 1991.
[13] S. Sinha, S. L. Lin, and J. N. Bardsley, "The mobility of $He^+$ ions in He," *J. Phys. B,* vol. 12, p. 1613, 1979.
[14] H. Helm, "The cross section for symmetric charge exchange of $He^+$ in He at energies between 0.3 to 8 eV," *J. Phys. B,* vol. 10, p. 3683, 1977.
[15] G. D. Alkhazov, "Effective cross sections for ionization and excitation of helium by electron impact," *Zh. Tekh. Fiz.,* vol. 40, p. 97, 1970.
[16] A. V. Phelps, "Absorption studies of helium metastable atoms and molecules," *Phys. Rev.,* vol. 99, p. 1307, 1955.
[17] W. C. Fon, K. A. Berrington, P. G. Burke, and A. E. Kingston, "Total cross sections for electron excitation transitions between the $1^1S, 2^3S, 2^1S, 2^3P$ and $2^1P$ states of atomic helium," *J. Phys. B,* vol. 14, p. 2921, 1981.
[18] A. Corney, *Atomic and Laser Spectroscopy,* Oxford: Clarendon Press, 1977.
[19] C. van Trigt, "Analytically solvable problems in radiative transfer," *Phys. Rev.,* vol. 181, p. 97, 1969.
[20] W. L. Wiese, M. W. Smith, and B. M. Glennon, *Atomic Transition Probabilities,* in Natl. Stand. Ref. Data Ser., Natl. Bur. Stand. (USA) Circ. 4, vol. I. Washington, D.C.: U.S. GPO, 1966.
[21] A. V. Phelps and J. P. Molnar, "Lifetimes of metastable states of noble gases," *Phys. Rev.,* vol. 89, p. 1202, 1953.

**W. N. G. Hitchon** Biography and photograph unavailable at time of publication.

**Gregory J. Parker** was born on August 5, 1967. He received his B.S. with Honors in physics and mathematics and his Ph.D. from the University of Wisconsin-Madison in 1989 and 1994, respectively. His dissertation was entitled "Propagator simulations of glow discharges." He is currently working at Lawrence Livermore National Laboratory in the Plasma Physics Research Institute doing computational studies of processing plasmas.

**J. E. Lawler** was born in St. Louis, Missouri, June 29, 1951. In 1973 he received a Bachelor of Science degree, Summa Cum Laude, from the University of Missouri at Rolla. As an undergraduate he performed research under the direction of Professor John T. Park on the U. M. R. Heavy Ion Energy Loss Spectrometer.

In 1974 he received a M.S. degree, and in 1978 he received a Doctor of Philosophy degree from the University of Wisconsin at Madison. His thesis title was "Dye Laser Studies of Pulsed High Pressure Gas Discharges," and his thesis advisor was Professor L. W. Anderson.

After leaving Wisconsin he worked as a Research Associate at Stanford University in the group of Professors Arthur L. Schawlow and Theo W. Hansch from 1978 to 1980. J. E. Lawler and his collaborators at Stanford developed new techniques for performing high resolution laser spectroscopy in gas discharge plasmas. These techniques for Doppler-free spectroscopy exploited sensitive optogalvanic detection.

J. E. Lawler returned to the University of Wisconsin as a faculty member in 1980. His current research interests are in two areas, both of which involve gas discharge plasmas and laser spectroscopy. He is developing and applying laser spectroscopic techniques for determining accurate absolute atomic transition probabilites. He is also using laser techniques to study gas discharge plasmas.

J. E. Lawler has received numerous fellowships including: a Schlumberger Scholarship and a Curators Waiver of Fees Award while at the University of Missouri, and a National Science Foundation Graduate Fellowship and a Wisconsin Alumni Research Foundation Graduate Fellowship while a student at Wisconsin. He is now a H. I. Romnes Faculty Fellow and Professor of Physics at the University of Wisconsin. He is a fellow of the American Physical Society, and a member of the Optical Society of America and Sigma Xi. He won the H. Q. Fuller Award from the University of Missouri. He won the 1992 W. P. Allis Prize of the American Physical Society.